International Journal of Mechanical Sciences 149 (2018) 150–163

Contents lists available at ScienceDirect

International Journal of Mechanical Sciences

journal homepage: www.elsevier.com/locate/ijmecsci

Design and strengthening mechanisms in hierarchical architected materials processed using additive manufacturing

Yin Sha[a,b], Li Jiani[a], Chen Haoyu[a], Robert O. Ritchie[c], Xu Jun[a,*]

[a] Advanced Vehicle Research Center (AVRC) & Department of Automotive Engineering, Beihang University, Beijing, China, 100191

[b] State Key Laboratory for Strength & Vibration of Mechanical Structures, School of Aerospace Engineering, Xi'an Jiaotong University, Xi'an, China, 710049

[c] Materials Sciences Division, Lawrence Berkeley National Laboratory, & Department of Materials Science & Engineering, University of California, Berkeley, CA 94720, USA

ARTICLE INFO

Keywords:
Architected materials
Bio-inspired materials
Lattice materials
Hierarchy
Nodal effect

ABSTRACT

Natural structural materials which feature hierarchical architectures, like bone and glass sponge skeletons, often display remarkable mechanical properties. Employing the principle of hierarchy can create self-similar architected metamaterials across multiple length-scales, but the strengthening mechanisms remain to be fully understood. In the present study, self-similar hierarchical octet-truss lattice materials were fabricated via additive manufacturing and deformed in uniaxial compression. Experimental results indicated that the mechanical properties of such hierarchical lattice materials were not determined by relative density, unlike those of non-hierarchical ones, but varied with strut slenderness ratios in the two hierarchical levels. In terms of specific strength and stiffness, hierarchical architected structures do not necessarily outperform non-hierarchical structures. To explain the underlying mechanisms of these phenomena, analytical models considering effects of complex nodal microstructure were established. The upper and lower bounds of strength for the hierarchical lattice materials were deduced and compared with that for the non-hierarchical materials; these comparisons suggested that the hierarchical construction could be used to access unique mechanical properties that are unachievable in traditional materials. Additional levels of hierarchy beyond the second order could be similarly analyzed. This study discerns how hierarchical architecture can be used to access the unique properties of lattice materials, provides insight into the role of design in regulating the mechanical properties of such mechanical metamaterials.

1. Introduction

Biological materials, such as cancellous bone, wood and radiolarians, exhibit excellent mechanical properties that benefit from their hierarchical microstructures [1, 2]. For example, cancellous bone, with its highly complex structure with up to seven hierarchical levels of organization, displays a dual function of structural support with impact protection [3]. Analogously, the Euplectella glass sponge has a hierarchical construction achieved through a lengthy evolution process and guided by environmental constraints; as such, it possesses exceptional mechanical stability and toughness [4].

Among corresponding synthetic structural materials, architected materials have attracted wide attention over the past decade; these include architected materials constructed with various constituents, including metallic [5], composite [6-8] and ceramic lattices [9], which have been processed by a wide variety of fabrication techniques to achieve desired mechanical properties. With the development of micro/nano fabrication, especially additive manufacturing, considerable attention has been focused on the development of micro-/nano-lattices. Specifically, electron beam melting [10-12] and selective laser melting [13-15] techniques have been used to rapidly manufacture micro-lattice materials of arbitrary shape. Yuan et al. [16] conducted a systematic investigation on the manufacturing process of selective laser sintering, including the optimization of the fabrication process and mechanical testing of 3D-printed structures. Compton et al. [17] reported a new epoxy-based ink that enabled 3D printing of cellular composites composed of oriented fiber-filled epoxy, and demonstrated the printed cellular composites with exceptional mechanical properties using experimental and theoretical methods. Additionally, stereolithography [18], self-propagating photopolymer waveguides [19-22], two-photon lithography and projection micro stereolithography techniques [23, 24] have also been developed to fabricate architected materials with complex geometries at micro to nano length-scales. Bauer et al. [25] have reviewed the progress that research has made into the topic of nanolattices as an emerging class of mechanical metamaterials, and expanded on the benefits of combining nanomaterials with lattice architectures. The mechanical properties

* Corresponding author.
E-mail address: junxu@buaa.edu.cn (X. Jun).

https://doi.org/10.1016/j.ijmecsci.2018.09.038
Received 26 July 2018; Received in revised form 24 August 2018; Accepted 24 September 2018
Available online 27 September 2018

Nomenclature

Q	repeating number of the 1st order octet-truss unit cell along the struts of the 2nd order octet-truss unit cell
$E_Z^{(2)}$	compressive stiffness of the 2nd order octet-truss unit cell
d_1	diameter of strut in the 1st order octet-truss lattice materials
$\lambda_{N_Q}^{(2)}$	modification of nodal volume effect of the larger strut
l_1	length of strut in the 1st order octet-truss lattice materials
$\lambda_{N_l}^{(2)}$	modification of nodal volume effect of the smaller strut
d_2	diameter of the smaller strut in the 2nd order octet-truss lattice materials
σ_I	buckling stress of the Type I struts
l_2	length of the smaller strut in the 2nd order octet-truss lattice materials
n	n is determined by the end condition of buckling strut; $n=1$ for pin-jointed strut, $n=2$ for fixed-end strut
$\bar{\rho}^{(1)}$	relative density of the 1st order octet-truss lattice materials
$\sigma_{buckling}^{(2)}$	strength of the 2nd order octet cell failing with Euler buckling of smaller strut
$\bar{\rho}^{(2)}$	relative density of the 2nd order octet-truss lattice materials
I_2	inertia moment of larger struts
E_S	compressive modulus of the parent nylon materials
$\sigma_{BUCKLING}^{(2)}$	strength of the 2nd order octet cell failing with Euler buckling of larger strut
σ_{ys}	compressive strength of the parent nylon materials
$\sigma_{yielding}^{(2)}$	strength of the 2nd order octet cell failing with plastic yielding
ε	strain
$F_A^{(1)}$	axial force of strut in the 1st order octet-truss lattice materials
δ_Z	imposed displacement of the 1st and 2nd order octet-truss lattice materials
$F_S^{(1)}$	sheer force of strut in the 1st order octet-truss lattice materials
δ_X	lateral deformation of the 1st and 2nd order octet-truss lattice materials along x axis
l_1'	equivalent length of the struts in the 1st order octet-truss lattice materials
δ_Y	lateral deformation of the 1st and 2nd order octet-truss lattice materials along y axis
I_1	inertia moment of struts in the 1st order octet-truss lattice materials
δ_A	axial deformation along the larger strut of the 2nd order octet-truss lattice materials
$P_T^{(1)}$	shear modification of Timoshenko beam
ω	inclination angle between the struts and the horizontal truss of the octet-truss unit cell
κ	shear coefficient
l_2'	equivalent length of the smaller struts in the 2nd order octet-truss lattice materials
G	shear modulus
Q'	equivalent repeating number of the 1st order octet-truss unit cell along the larger strut of the 2nd order octet-truss unit cell
A_1	cross-section area of struts in the 1st order octet-truss lattice materials
δ_α	axial deformation along each substructure in the larger strut of the 2nd order octet-truss unit cell
ν	Poisson's ratio of nylon material
θ_1	inclination angle between the Type I struts and the axial direction of corresponding larger strut
$E_Z^{(1)}$	compressive stiffness of the 1st order octet-truss lattice materials
θ_2	inclination angle between the Type II struts and the axial direction of corresponding larger strut
$\lambda_V^{(1)}$	modification of nodal volume effect in the 1st order octet-truss lattice materials
θ_3	inclination angle between the Type III struts and the axial direction of corresponding larger strut
$\lambda_B^{(1)}$	modification of bending volume effect in the 1st order octet-truss lattice materials
F_I	axial force in the Type I struts
$\sigma_{buckling}^{(1)}$	strength of the 1st order octet cell failing with Euler buckling
F_{II}	axial force in the Type II struts
$\sigma_{yielding}^{(1)}$	strength of the 1st order octet cell failing with plastic yielding
F_{III}	axial force in the Type III struts

of these materials depend on their constituent materials, their architecture or combinations of the two.

Inspired by biological materials in Nature, architected materials with multiple hierarchical levels have been designed across different length-scales and studied for their effects on mechanical behavior [26-30]. The design concept of recursion has been widely applied to create hierarchical architected materials through the topology of lower-order unit cell [31–33]. Meza et al. [34] investigated the effect of structural hierarchy on the stiffness, strength and resilience[1] of nanolattices using nanomechanical experiments and computer modeling. They found that more than two levels of hierarchy would not stiffen or strengthen these structures but would help to amplify their recoverability. Zheng et al. [24] developed hierarchical metamaterials with various three-dimensional features spanning seven orders of magnitude, which exhibited high tensile ductility with tensile strains approaching 20%, behavior not found in their brittle-like metallic constituents. However, the fundamental mechanisms underlying this behavior across different length-scales were not made clear.

In general, the increase of hierarchical level would introduce complexity on lattice nodes and mechanical behavior of architected materials. Detailed analytical models considering the node complexity were absent to evaluate effects of hierarchical level and structural parameters. Also, how to manipulate mechanical properties by adjusting the microstructures was still unknown. To bridge this gap, the current work will be carried out as followed. Specifically, we fabricate self-similar hierarchical octet-truss architected materials using additive manufacturing, characterize their uniaxial mechanical response through experiments and theoretical modeling, and compare their mechanical behavior to that in non-hierarchical architected materials. The key factors that govern mechanical properties of hierarchical constructions are explored with the objective of discerning their structural efficiencies.

2. Design and fabrication

An octet-truss (termed as face-centered cubic, fcc) unit cell is composed of a central octahedral cell with 12 struts and 8 edge tetrahedrons

[1] Resilience means sample's recoverability, defined as the height after unloading divided by its original height, as described by Meza et al. [25].

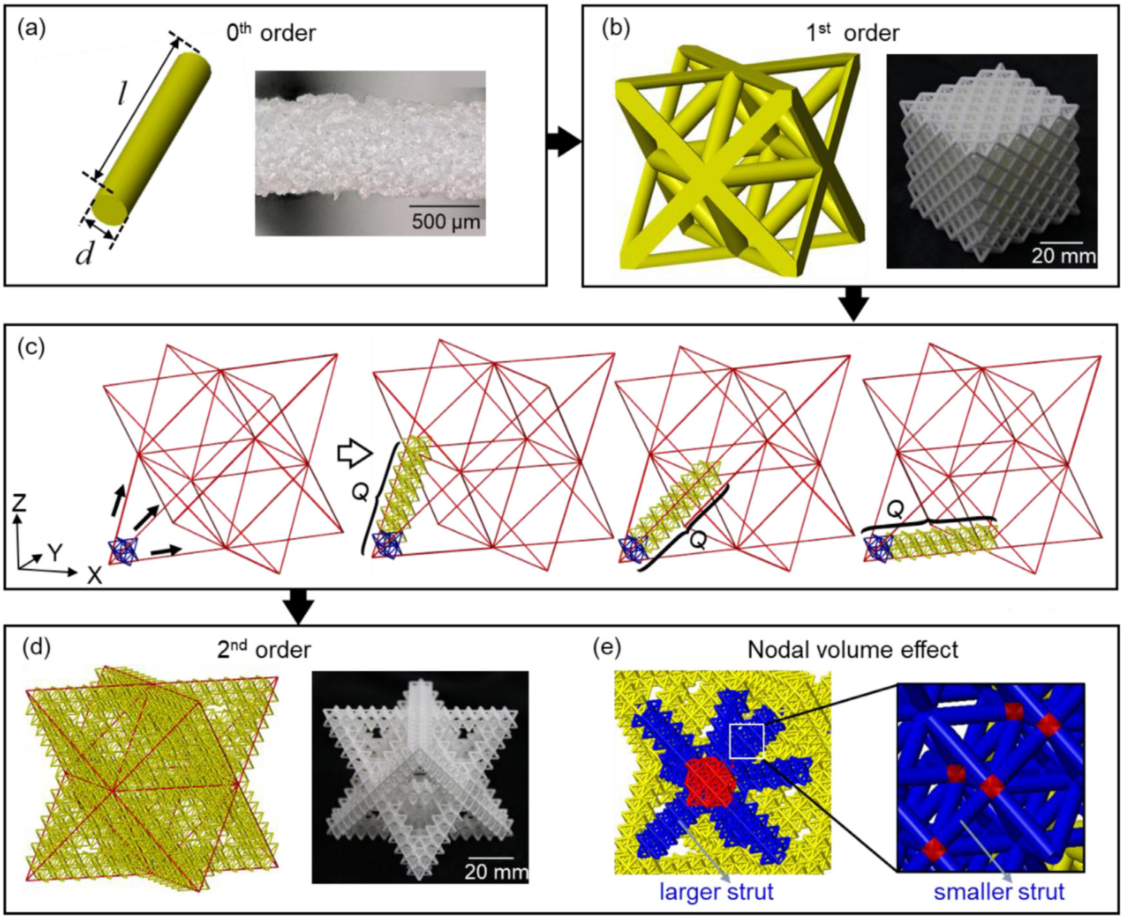

Fig. 1. Computer-aided design (CAD) of hierarchical octet-truss lattice materials and specimens fabricated by selective laser sintering. (a) a zero-order repeating truss unit; (b) a first-order octet-truss unit; (c) illustration about the patterning method for (d) a second-order hierarchical octet-truss unit cell; (e) nodal volume effects arising from the complex microstructure and coincident volume at the nodes formed by larger or smaller truss members.

each with 3 struts. The octet-truss unit cell possesses a nodal connectivity of 12 which satisfies Maxwell's rigidity criterion, and thus will deform according to a stretch-dominated mechanism [35] . A hierarchical octet-truss architected material is designed using a recursive method as shown in Fig. 1. Specifically, an octet-truss unit (Fig. 1b) is patterned along the truss length direction (Fig. 1c), with topological interval of half a unit cell and repeating number of Q, resulting in a fractal-like 2nd order self-similar geometry (Fig. 1d). Note that during this construction, the local coordinate system of the 1st order octet-truss unit cell is kept the same as that of the 2nd order. These steps can be repeated iteratively to create hierarchical lattice materials of any order; indeed, the method is sufficiently general that it can be repeated for a wide range of unit cell geometries.

Selective laser sintering (SLS) was employed for the manufacture of all samples in this study using an additive manufacturing machine (EOS P396, Germany) with polyamide PA 2200 powder (Nylon 12). The system begins by applying a thin layer of powder material to the building platform. Subsequently, the powder is selectively fused by powerful laser beam and solidified according to the sample geometry. Samples were fabricated together in 6 hr or less without any supporting structures which are often difficult to remove. Photographs of the printed non-hierarchical and hierarchical lattice materials are shown in Figs. 1b and 1d, respectively. From the surface tomography image of a single truss (Fig. 1a), taken with a Keyence VHX-6000 optical microscope, the powder can be seen to have sintered thoroughly; the truss diameter appears to be slightly varied, which can be attributed to the fabrication process, in particular the slicing method, powder thickness and accuracy of electronic scanning. By changing the strut slenderness ratio, *i.e.*, the ratio of length to diameter of the struts, four groups of non-hierarchical counterparts of $5 \times 5 \times 5$ unit cells were obtained, respectively termed as A1-A4 for comparison; correspondingly, six groups of hierarchical octet-truss unit cells, termed as B1-B6, were fabricated with the same slenderness ratio and variable unit repeating numbers Q. The geometries are summarized in Table 1, and the overall dimension of all specimens is $56 \times 56 \times 56$ mm. Note that the strut diameter is restrained by the smallest achievable feature size of the present additive manufacturing machine.

For non-hierarchical octet-truss lattice materials, the relative density has been derived previously [35] as $\bar{\rho}^{(1)} = \frac{3\sqrt{2}\pi}{2}(\frac{d_1}{l_1})^2$, where d_1 and l_1 are lattice truss diameter and length. However, for those with higher relative densities (> 0.1), the coincident volume at the joints of the lattice members must be taken into account [36]. A curve fit of the relative densities calculated by CAD models of Groups A1-A4 suggests adding a cubic correction [10], given as:

$$\bar{\rho}^{(1)} = \frac{3\sqrt{2}\pi}{2}\left(\frac{d_1}{l_1}\right)^2 - 6.825\left(\frac{d_1}{l_1}\right)^3, \tag{1}$$

For hierarchical lattice materials, larger lattice struts consisting of octet-truss cells will form super nodes with complex microstructure at the joints, as shown in Fig. 1e. Nodal volume effects should be considered because of the coincident volume at each node, both with larger and smaller struts. Similarly, the relative density of the 2nd order hierarchical octet-truss unit cell, $\bar{\rho}^{(2)}$, can be calculated in terms of the relative density of octet-truss unit cell times that of the substructure in its larger

Table 1
Summary for geometries of the 1st order and 2nd order octet-truss lattice materials.

Specimen	d_1 (mm)	l_1 (mm)	d_1/l_1	$\bar{\rho}^{(1)}$ Theoretical value (Eq.1)	Actual value
A1	1.28	7.92	0.1616	0.15	0.15
A2	1.60	7.92	0.2020	0.22	0.23
A3	1.92	7.92	0.2424	0.29	0.32
A4	2.24	7.92	0.2828	0.38	0.42

Specimen	Q	d_2 (mm)	l_2 (mm)	d_2/l_2	$\bar{\rho}^{(2)}$ Theoretical value (Eq.2)	Actual value
B1		0.8	4.95	0.1616	0.06	0.05
B2	8	1.0	4.95	0.2020	0.09	0.08
B3		1.2	4.95	0.2424	0.12	0.12
B4		1.4	4.95	0.2828	0.16	0.16
B5	6	1.0	4.95	0.2020	0.13	0.12
B6	10	1.0	4.95	0.2020	0.06	0.05

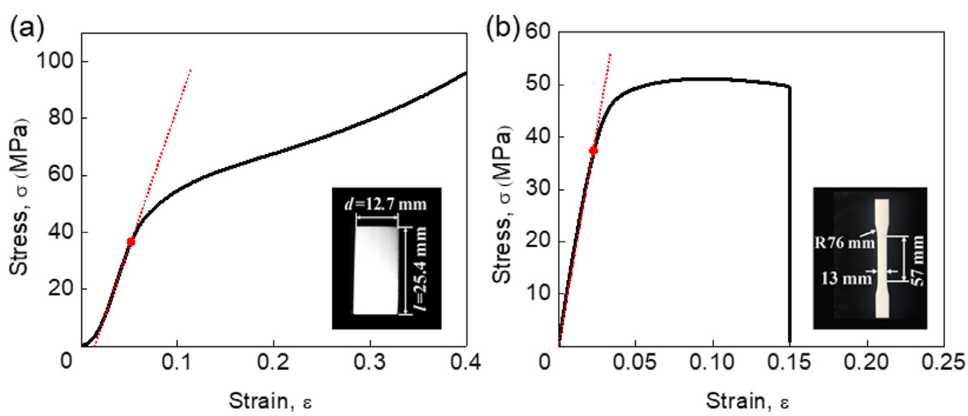

Fig. 2. (a) Compressive and (b) tensile engineering stress-strain curves of the constitutive nylon materials.

strut as:

$$\bar{\rho}^{(2)} = \frac{36Q-92}{Q^3}\left[\frac{25\sqrt{2}\pi}{16}\left(\frac{d_2}{l_2}\right)^2 - 5.922\left(\frac{d_2}{l_2}\right)^3\right] \tag{2}$$

where d_2 and l_2 are diameter and length of the smaller struts. The measured relative densities agree well with those obtained by theoretical prediction, as indicated in Table 1.

3. Experiments

Quasi-static compression tests for the hierarchical lattice materials were carried out and their compressive behavior analyzed and compared with those of non-hierarchical counterparts. All the specimens were compressed on a servo-hydraulic testing machine (Instron 8801) equipped with two parallel high strength steel loading platens, at a constant cross-head strain rate of about 10^{-3}/s. The compression force was read from the load cell, while the compressive displacement was measured using a laser extensometer. Three tests were carried out for each group of specimens to ensure repeatability. Also, the compressive and tensile properties of the parent constitutive material were tested.

3.1. Compressive response of constitutive materials

The compressive and tensile stress-strain curves of the constitutive nylon materials, which were made by 3D printing in accordance with ASTM D695-15 [37] and ASTM D638-14 [38], are shown in Fig. 2. For the compressive test, a linear-elastic stage appeared first, then the cylindrical strut starts to yield followed by nonlinear strain-hardening behavior. For the tensile test, after an initial linear-elastic stage, the slope decreases gradually with the dog-bone shaped specimen entering its "plastic" stage until the curve starts to fall rapidly. The slopes of the linear stages are considered to be the modulus and the values of the stress at the *y*-axis, defined by the end point of linear-elastic stage, were taken as the yield strength. The calculated values of the compressive modulus E_S, compressive yield strength σ_{ys}, tensile modulus $E_S{'}$ and tensile yield strength $\sigma_{ys}{'}$, were 1180 MPa, 37.5 MPa, 1662 MPa and 39.9 MPa, respectively.

3.2. Compressive response of non-hierarchical lattice materials (1st order)

The compressive stress–strain curves of the 1st order lattice material are shown in Fig. 3 together with the deformation modes. Representative compressive responses were typical of cellular materials exhibiting high frequency oscillations.

For Group A1 ($\bar{\rho}^{(1)} = 0.15$), a linear-elastic stage appeared first, reaching a peak followed by a sharp drop, before subsequently strain hardening prior to densification. The oscillation in the stress-strain curve was due to a layer-by-layer collapse. As shown in Fig. 3b, the onset of failure appeared first at the boundary layer by Euler buckling of lattice members, followed by progressive crushing towards the specimen center; this behavior has been widely observed for other conventional cellular solids.

For Groups A2 and A3, after deforming in a linear-elastic manner, the experimentally-measured macroscopic engineering stress-strain curve becomes non-linear, reaching the first stress peak while the deformation fields were still macroscopically uniform. After the peak, the stress decreased slowly, accompanied by yielding and fracture of the structure, before diagonal crushing, as shown in Fig. 3c-d.

For Group A4 with relative density of 0.42, no sharp stress drops were observed but instead a clear stress plateau stage appeared after the peak followed by small stress fluctuations until densification. Shear localization bands were created which triggered strut plastic yielding and

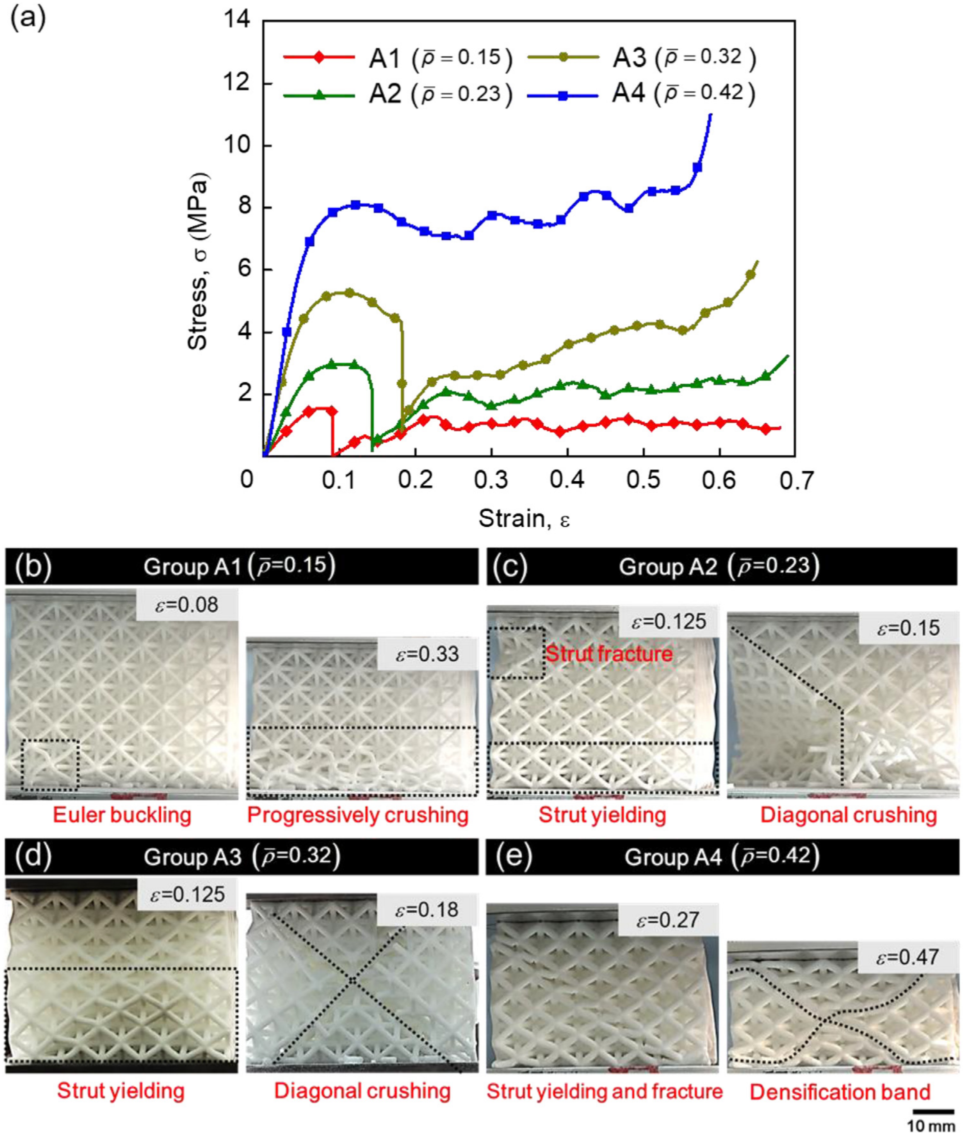

Fig. 3. (a) Compressive stress-strain curves and the corresponding deformation histories of the 1st order octet-truss lattice materials with relative densities of (b) 0.15, (c) 0.23, (d) 0.32 and (e) 0.42.

fracture along the diagonals, followed by subsequently densification, as shown in Fig. 3e. Note that similar localization densification bands were observed for metallic fcc metamaterials in a previous study [10]. For specimens in Groups A3-A4 with larger relative densities, the mesoscopic deformation mode was in the form of plastic hinges which were created near the strut nodes before nodal rupture and sample crushing; accordingly, bending deformation could not be neglected during theoretical analysis, as discussed in the Appendix B.

3.3. Compressive response of hierarchical lattice materials (2nd order)

For the 2nd order lattice materials, the compressive stress-strain curves for six groups of specimens were shown in Fig. 4a. The curves exhibited two obvious peaks during compression because the lower and upper half-cells failed progressively as the strain increased, and the horizontal larger struts did not deform. The deformation process of Group B4 ($\bar{\rho}^{(2)} = 0.16$), for example, is shown in Fig. 4b. Referring to the corresponding stress-strain curve, after the linear-elastic stage the stress-strain curve became non-linear and reached the first stress peak at ~0.96 MPa accompanied by buckling of larger struts in the lower half-cell. As the strain increased, the upper half-cell started to deform after the lower one fully collapsed, at a strain of 0.3; the latter buckled at the second stress peak followed by its full collapse at a strain of ~0.45 prior to densification. Additionally, more possible failure modes appeared for the hierarchical materials. The representative failure modes could be Euler buckling of smaller lattice strut (Group B1), plastic yielding (Group B5), and macroscopic Euler buckling of larger strut, as summarized in Fig. 4c.

4. Theoretical analysis

As the length-scale is diminished, material size effects and primarily architectural effects begin to play a competing role on mechanical properties of architected materials (e.g., nanolattices) depending on their relative density [25]. Here, we only focus on mechanisms of hierarchical architecture for these materials whatever the length-scale is.

The compressive stiffness and strength prediction formulae are deduced for the 2nd order hierarchical octet-truss unit cell similarly as those for non-hierarchical lattice materials [36], which are derived in the Appendix B. To facilitate our analysis, a single larger strut of the hierarchical octet-truss unit cell is extracted, as shown in Fig. 5. All the lattice members are presumed to be compressed with pin-jointed

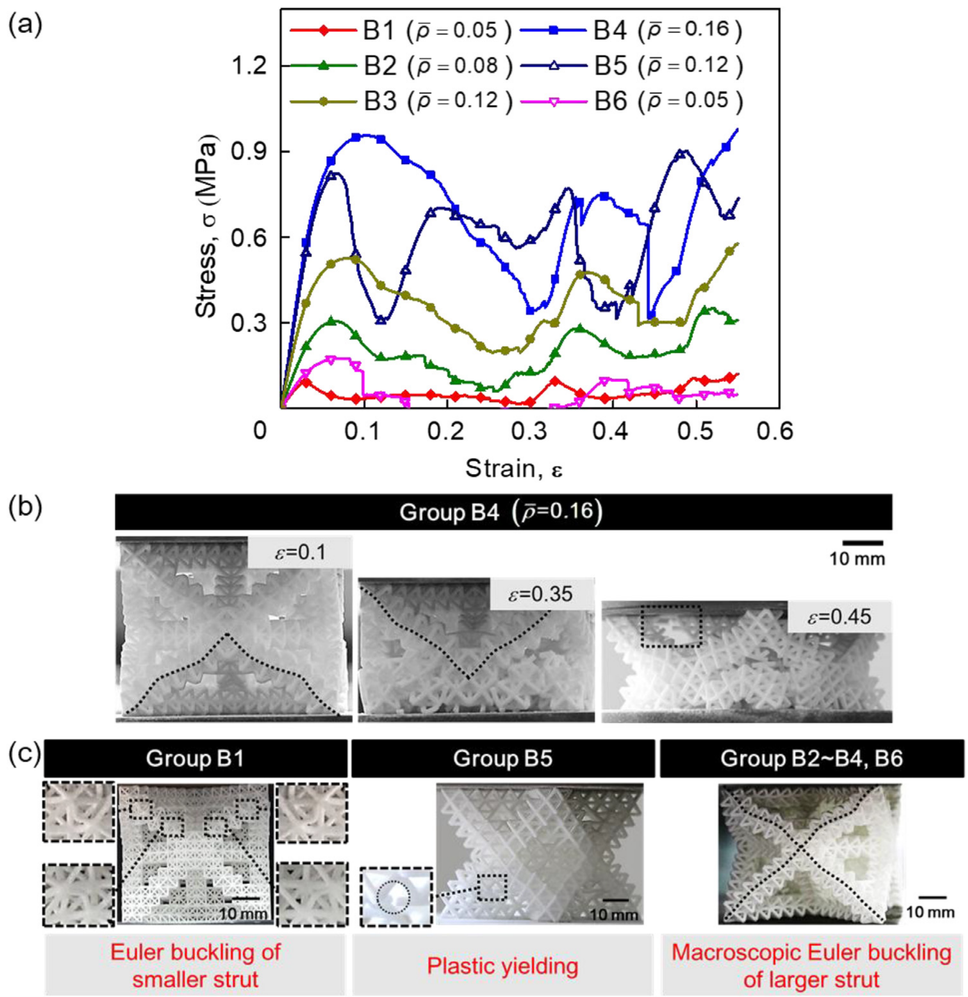

Fig. 4. (a) Compressive stress-strain curves of the 2nd order octet-truss lattice materials with relative densities of 0.05, 0.08, 0.12, 0.16, 0.12 and 0.05; (b) typical failure modes that were observed; and (c) deformation histories for the 2nd order octet-truss lattice materials with relative densities of 0.16.

ends, thus ignoring any small bending deformation. For hierarchical lattice materials, the effect of nodal volume is clear due to the complex microstructure at the nodes (Fig. 1e), which need to be considered in any theoretical analysis. Here, nodal volume effects of both larger and smaller lattice members are considered by introducing equivalent cell number Q' (Fig. 5c-d) and smaller strut length l_2' (Fig. 5e-f), respectively. For the imposed displacement δ_Z in the z-direction shown in Fig. 5a, the lateral deformation due to effects of Poisson's ratio leads to $\delta_X = \delta_Z/3$, such that the axial deformation along the secondary strut becomes $\delta_A = \delta_Z \sin\omega - \delta_X \cos\omega$, where ω=45° for the fcc construction.

4.1. Stiffness

The representative substructure in the larger strut is shown in Fig. 5d. For this configuration, the axial deformation along each substructure is $\delta_\alpha = \delta_A/2Q'$. Three types of struts exist in the substructure, and the corresponding strut inclination angles are defined according to the loading direction with $\theta_1 = 0^{\circ}$, $\theta_2 = 90^{\circ}$ and $\theta_3 = 60^{\circ}$. Using truss system analysis theory [39], the corresponding axial forces in three types of struts are respectively: $F_I = \pi d_2^2 E_S \delta_\alpha \cos\theta_1 / 4 l_2' \cos\theta_3$, $F_{II} = 0$ and $F_I = \pi d_2^2 E_S \delta_\alpha \cos\theta_3 / 4 l_2'$. Thus, the compressive stiffness of the 2nd order hierarchical octet-truss unit cell can be expressed as:

$$E_Z^{(2)} = \frac{5\sqrt{2}\pi E_S}{4} \left(\frac{d_2}{Q l_2} \right)^2 \lambda_{N_Q}^{(2)} \lambda_{N_l}^{(2)}, \tag{3}$$

where the two parameters $\lambda_{N_Q}^{(2)} = Q/Q'$ and $\lambda_{N_l}^{(2)} = l_2/l_2'$, represent contributions of nodal volume effects of the larger and smaller struts, respectively. Note that only axial deformation is considered in the above analysis, and the contribution from strut bending deformation (termed as bending effects) on compressive properties are neglected to simplify the analysis.

4.2. Strength

More possible failure modes exist in the hierarchical octet-truss lattice material during uniaxial compression, namely (i) Euler bucking of the smaller struts (EB1), (ii) macroscopic Euler buckling of the larger struts (EB2), and (iii) strut plastic yielding (PY). We now provide below predictive models for each of these failure modes.

(1) Euler buckling of the smaller struts

During compression, the Type I struts always fail prior to the Type II and III struts. Accordingly, the buckling stress in smaller strut is $\sigma_I = n^2\pi^2 E_S d_2^2 / 16 l_2'^2$ with n = 1, and the corresponding strength of the 2nd order hierarchical octet cell will be:

$$\sigma_{buckling}^{(2)} = \frac{15\sqrt{2}\pi^3 E_S}{64 Q^2} \left(\frac{d_2}{l_2} \right)^4 \lambda_{N_Q}^{(2)} \left(\lambda_{N_l}^{(2)} \right)^2. \tag{4}$$

Note that because the modification of Q′ in $\lambda_{N_Q}^{(2)}$ can be offset; $\lambda_{N_Q}^{(2)}$ will be equal to unity in the expression for $\sigma_{buckling}^{(2)}$ in Eq. 4.

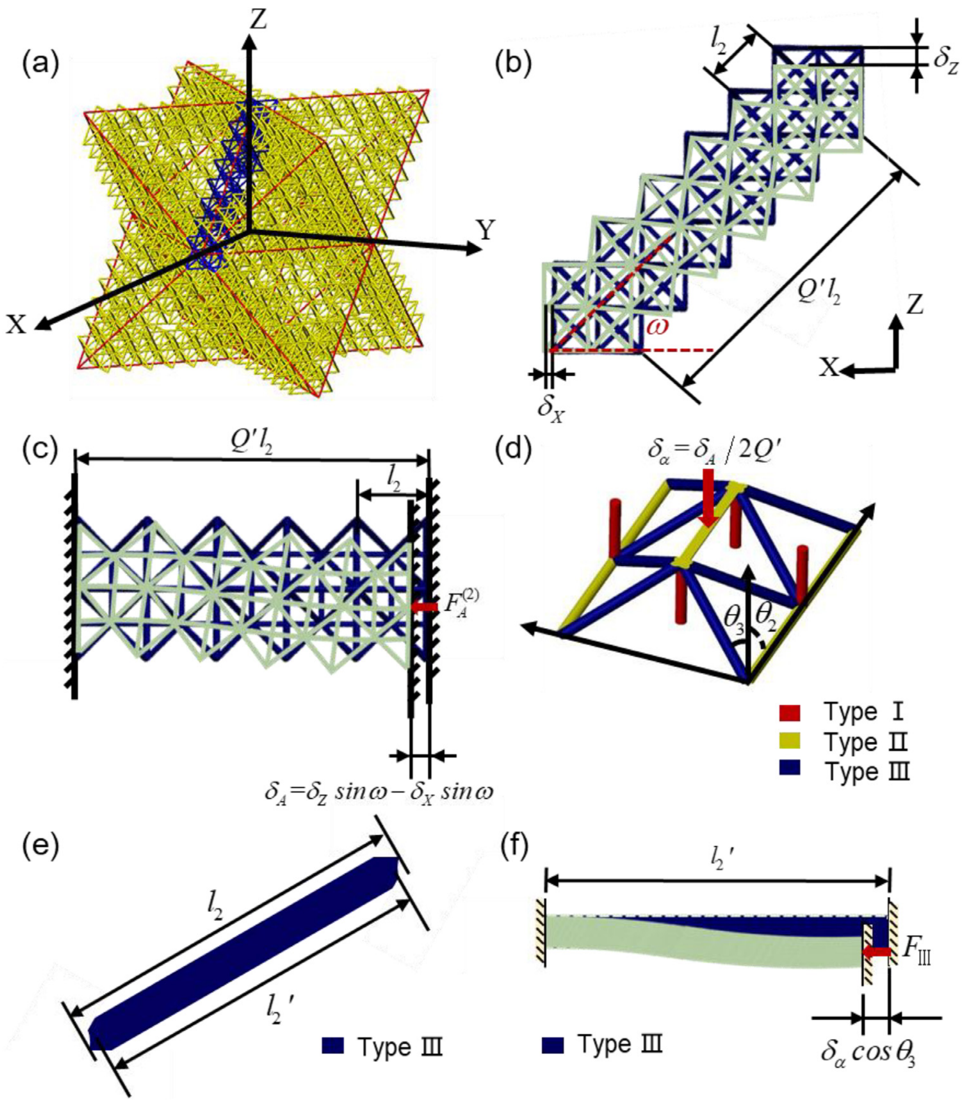

Fig. 5. (a-c) Free-body diagram of a single larger strut for the hierarchical lattice material under uniaxial compression; (d) the representative substructure in the larger strut; (e) equivalent length of Type III struts considering nodal effects; (f) deformation sketch of Type III strut.

(1) Euler buckling of the larger struts

The inertia moment of the larger struts determines their buckling resistance, simplified here as that of the Type I struts (Fig. 5d), i.e., as $I_2 = \pi d_2^2(d_2^2+2l_2^2)/16$. Thus, the collapse strength for failure by Euler buckling of a larger strut can be derived as:

$$\sigma_{BUCKLING}^{(2)} = \frac{3\sqrt{2}\pi^3 E_S d_2^2 \left(d_2^2+2l_2^2\right)}{16Q^4 l_2^4}\left(\lambda_{N_Q}^{(2)}\right)^2 \lambda_{N_l}^{(2)}. \tag{5}$$

Note that the nodal volume effect of smaller strut $\lambda_{N_l}^{(2)}$ equals unity in Eq. 5.

(1) Plastic yielding

If the strut fails by plastic yielding, then $\sigma_I = \sigma_{ys}$, and thus the compressive strength of the 2nd order octet cell is:

$$\sigma_{yielding}^{(2)} = \frac{15\sqrt{2}\pi d_2^2}{4Q^2 l_2^2}\sigma_{ys}\lambda_{N_Q}^{(2)}\lambda_{N_l}^{(2)}. \tag{6}$$

Here, both $\lambda_{N_Q}^{(2)}$ and $\lambda_{N_l}^{(2)}$ will be equal to unity and thus nodal volume effects can be ignored when plastic yielding occurs.

5. Discussion

5.1. Compressive stiffness and strength

Experimental stiffness and strength values are plotted and compared with different prediction models for both the hierarchical and non-hierarchical octet-truss lattice materials in Fig. 6. All the specific values are summarized in Table C1 and C2, and more detailed compared results between theoretical and experimental values were clarified in Appendix C. With the same geometry of d/l ($d_1/l_1 = d_2/l_2$), the compressive performance and failure modes of the two types of lattice materials can be seen to be totally different. Effects of structural geometries on compressive properties for both non-hierarchical and hierarchical lattice materials are discussed below.

For the non-hierarchical octet-truss lattice materials, theoretical models are plotted as a function of strut slenderness ratio, d_1/l_1, as shown in Fig. 6a, to explore the effect of this ratio on the selection of the appropriate predictive models. Specifically, four types of stiffness mod-

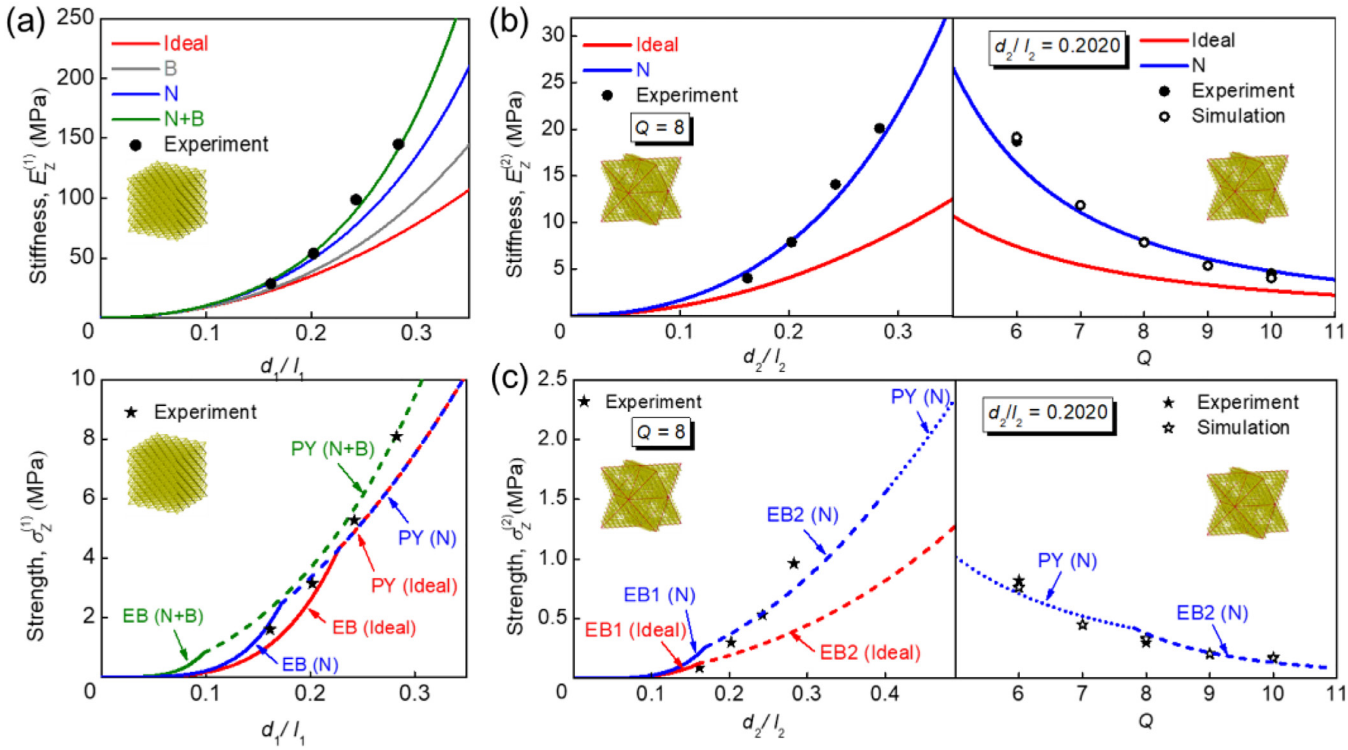

Fig. 6. Variation of compressive stiffness and strength with the geometries examined. (a) Effects of d_1/l_1 on the compressive properties of the non-hierarchical 1st order octet-truss lattice materials; effects of d_2/l_2 and Q on (b) the compressive stiffness and (c) the strength of the second-order hierarchical octet-truss lattice materials. EB: Euler buckling; PY: plastic yield; N: models considering nodal volume effect; B: models considering bending effect; N + B: models considering both nodal volume and bending effects; Ideal: models considering neither nodal or bending effect.

els and six types of strength models are plotted. By comparison to experimental data, nodal volume and bending deformation effects can be considered selectively at different d_1/l_1. From Fig. 6a, we can directly find that for non-hierarchical octet-truss lattice materials, the nodal volume effect contributes more than the bending effect to stiffness; meanwhile, the latter one does not cause much variation in strength experimentally, which actually is contrary to the prediction by molecular dynamics simulations for nanolattices [36].

For hierarchical octet-truss lattice materials, the compressive stiffness and strength are plotted as functions of two governing geometrical parameters, d_2/l_2 of the smaller struts and the repeating unit numbers in the larger struts, respectively. Note that structures with more possible Q values as the geometrical variable are virtually tested by simulation (see Appendix D), and the corresponding stiffness and strength values are summarized in Figs. 6b-c. Two types of stiffness models and five types of strength models are plotted and compared with experimental values. Overall, the stiffness and strength models that consider the nodal volume effect can improve the accuracy of prediction.

5.2. Effects of hierarchical level

The specific stiffness $E_Z^{(2)}/\bar{\rho}^{(2)}$ and specific strength $\sigma_Z^{(2)}/\bar{\rho}^{(2)}$ of the 2nd order hierarchical lattice materials are compared with those of the non-hierarchical lattice materials in Fig. 7. Note that the relative densities of B1 and B3 are respectively the same as those of B6 and B5, even though the geometrical parameters $d2/l2$ and Q are different. Accordingly, the specific stiffness and strength can have different values at the same relative density, which means that the mechanical properties depend directly on the geometry of the two structural levels and not on their relative density. We can also see from Fig. 7 that the specific stiffness and strength of the 2nd order hierarchical lattice materials do not outperform those of the non-hierarchical ones as expected. Accordingly, the design and strengthening mechanisms of hierarchical constructions require further examination, as described below.

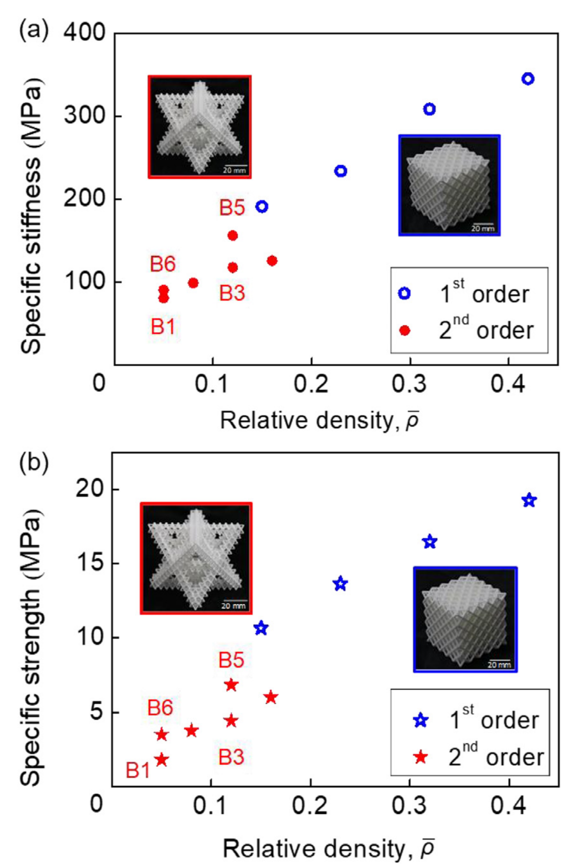

Fig. 7. Effects of hierarchihcal level on (a) specific stiffness and (b) specific strength of lattice materials as a function of their relative density.

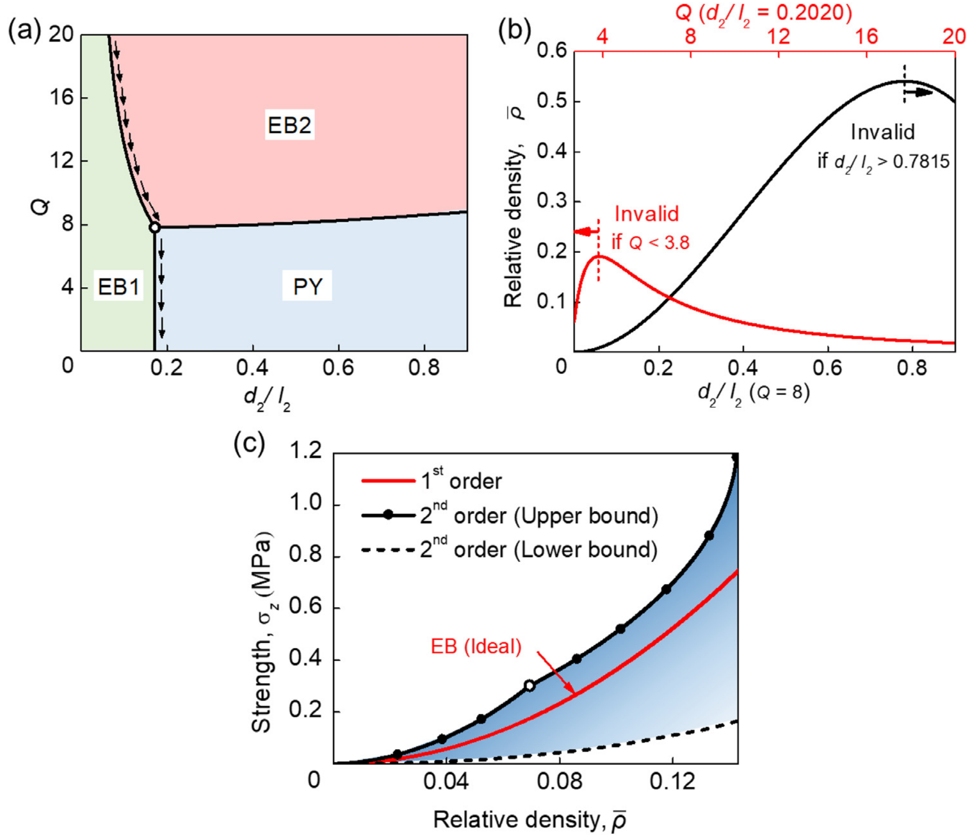

Fig. 8. (a) A collapse mechanism map for the 2nd order octet-truss lattice materials with arrows indicating the optimal pathways that maximize compressive strength at a given relative density; (b) variation of relative density with d_2/l_2 (Q=8) and Q (d_2/l_2=0.2020) respectively; (c) the relationships between the optimized (upper) and minimum (lower) strength bounds of the hierarchical lattice materials with their relative densities, as compared with those of non-hierarchical ones.

5.3. Optimization

A collapse mechanism map is constructed for the 2nd order hierarchical octet-truss lattice materials in Fig. 8a, and indicates the various predicted collapse modes as a function of the geometrical parameters d_2/l_2 and Q. The boundaries of each collapse regime were obtained by equating the predicted collapse strength (Eqs. 4-6), with consideration of the nodal volume effect, for each mode in turn. This map can serve as a guide for the design and development of hierarchical lattice materials for structural efficiency coupled with minimum weight [40, 41]. The arrows in Fig. 8a indicate the various pathways for optimal designs that maximize the compressive strength of hierarchical structures at a given relative density, represented by:

$$\begin{cases} Q = \sqrt{0.8 \times \left[1 + 2\left(l_2/d_2\right)^2\right] \times \left[1 - \sqrt{2}\left(d_2/l_2\right)\right]^2} + 2.2, \\ \qquad \text{along EB1 } - \text{EB2 boundary as } Q \geq Q_0 \\ \frac{d_2}{l_2} = 1/\left(\sqrt{\pi^2 E_S/\left(16\sigma_{ys}\right)} + \sqrt{2}\right), \text{alongEB1} - \text{PYboundaryas} Q < Q_0 \end{cases}, \tag{7}$$

where $Q_0 = \sqrt{0.8 \times [1 + 2(\sqrt{\pi^2 E_S/(16\sigma_{ys})} + \sqrt{2})^2] \times [1 - \sqrt{2}(1/(\sqrt{\pi^2 E_S/(16\sigma_{ys})} + \sqrt{2}))]^2} + 2.2$. Thus, the upper bound of compressive strength is obtained. Subsequently, the minimum strength bound is found with Eqs. 2, 4-6 using a numerical approach at each specific relative density.

The upper and lower bounds of compressive strength will be plotted as a function of the relative densities. However, if we revisit the model predictions for the relative density in Eq. 2, the relative density $\bar{\rho}^{(2)} \sim \bar{\rho}^{(2)}(d_2/l_2, Q)$ increases first and then decrease as d_2/l_2 increases or Q is reduced as shown in Fig. 8b. This abnormal phenomenon is attributed to the extremely large nodal volume as $d_2/l_2 > 0.7851$ or $Q < 3.8$ when the lattice material is almost completely dense; under these conditions, the predicted model in Eq. 2 becomes invalid. Accordingly, results are plotted in Fig. 8c as a function of the relative density in regimes where the models (Eq. 2) are valid ($\bar{\rho}^{(2)} < 0.15$).

The maximum and minimum strength values of the 2nd order hierarchical lattice materials are also compared with those for the non-hierarchical lattice materials in Fig. 8c. For a given relative density, manipulate mechanical properties by adjusting the microstructures. Accordingly, one can perceive that this hierarchical strategy could be used to access unique mechanical properties that are unachievable in traditional materials.

6. Conclusions

Inspired by hierarchical structure of many biological and natural materials, hierarchical octet-truss lattice materials have been designed in this study and manufactured using selective laser sintering. Specifically, we examined the uniaxial quasi-static compressive mechanical performance of the second-order hierarchical octet-truss lattice materials with different geometries, and compared their behavior with that of the non-hierarchical materials. Our rationale was to identify the salient mechanistic deformation and failure modes in such hierarchical architected materials such that they can be developed to provide superior mechanical performance to non-hierarchical architected materials. Based on this work, the following conclusions can be made:

- The compressive performance was totally different as the hierarchical level increased; in particular, more possible failure modes were apparent.
- Analytical models considering the coincident volume at complex nodal microstructures were established for the compressive stiffness

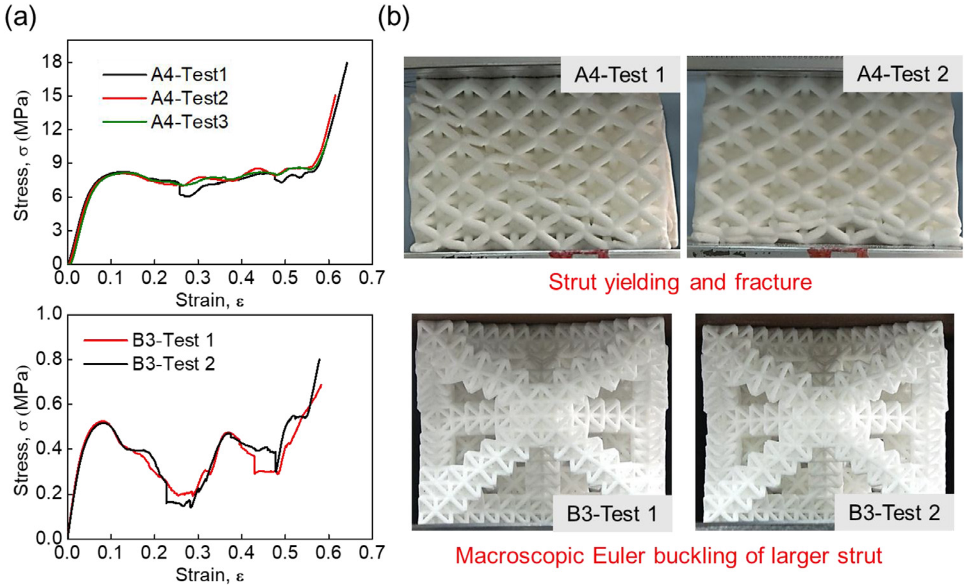

Fig. A1. (a) Compressive stress-strain curves and (b) the corresponding failure modes of the repeated experiments of A4 and B3.

and strength of the hierarchical lattice materials; predicted values of stiffness and strength agreed well with experimental values.

- Unlike the power-law rule between stiffness/strength and relative density for non-hierarchical lattice materials, the mechanical properties of hierarchical lattice materials were not determined by the relative density, but instead varied with strut slenderness ratios at the two structural levels.
- Collapse mechanism maps were constructed to display the upper and lower bounds of strength for the second-order hierarchical lattice materials; these bounds were, respectively, superior and inferior to those for the non-hierarchical lattice materials. Accordingly, we believe that this hierarchical strategy with cautious selection of strut slenderness ratios at each hierarchical level, can be used to access unique mechanical properties that are unachievable in traditional materials.

In general, we find that the mechanical properties of such architected lattice materials are determined by their architecture. We trust that the salient mechanisms of deformation and failure that we observe and model for our lattice materials in this work, will provide guidelines for the next-generation design and development of superior mechanical metamaterials with unprecedented mechanical properties to meet the requirements of the ever-demanding structural applications of the future.

Acknowledgements

This work was financially supported by the National Natural Science Foundation of China under grant No. U1664250, the National Key Research and Development Program of China, (2017YFB0103703), Young Elite Scientist Sponsorship Program by CAST, and Opening fund of State Key Laboratory for Strength and Vibration of Mechanical Structures, Xi'an Jiaotong University (SV2016-KF-20). ROR was supported by the U.S. Department of Energy, Office of Science, Office of Basic Energy Sciences, Materials Sciences and Engineering Division, under contract no. DE-AC02-05CH11231.

Appendix A. Repeatability of the compressive experiments

Repeated tests of groups A1-A4 and B1-B6 have been conducted to explore the consistency of the experiments. The compressive stress-strain curves and the corresponding failure modes of the repeated experiments of Group A4 and Group B3 are shown in Fig. A1. It can be observed that the elastic stage and peak force keep the same among the repeated tests, while the curves after the peak show a slight difference. Besides, for different repeated tests, the failure mode remains unchanged but the failure location does vary which might due to the random printing defects at micro-scales.

Appendix B. Compressive properties of the non-hierarchical octet-truss unit

Due to fabrication limitation, only hierarchical octet-truss lattice unit could be obtained with the printing technology in this study. Correspondingly, four groups of the non-hierarchical octet-truss lattice unit cell (1st order), termed as C1-C4, were fabricated with the same slenderness ratio and overall dimension as A1-A4, to examine cell number effect. The geometries and compressive properties of C1-C4 are summarized in Table B1. Also, the compressive stress–strain curves of C1-C4 are shown in Fig. B1 together with corresponding deformation modes. By comparing the stiffness, strength and failure mode of C1-C4 with

Table B1
Summary for geometries and compressive properties of the 1st order octet-truss lattice unit cell.

Specimen	d_1 (mm)	l_1 (mm)	d_1/l_1	Stiffness (MPa)	Strength (MPa)	Deviation percentage from A1-A4	
						Stiffness	Strength
C1	6.40	39.60	0.1616	37.71	1.92	24.16%	16.67%
C2	8.00	39.60	0.2020	61.43	3.22	12.58%	2.48%
C3	9.60	39.60	0.2424	86.62	4.94	12.24%	6.68%
C4	11.20	39.60	0.2828	122.60	6.81	18.27%	18.80%

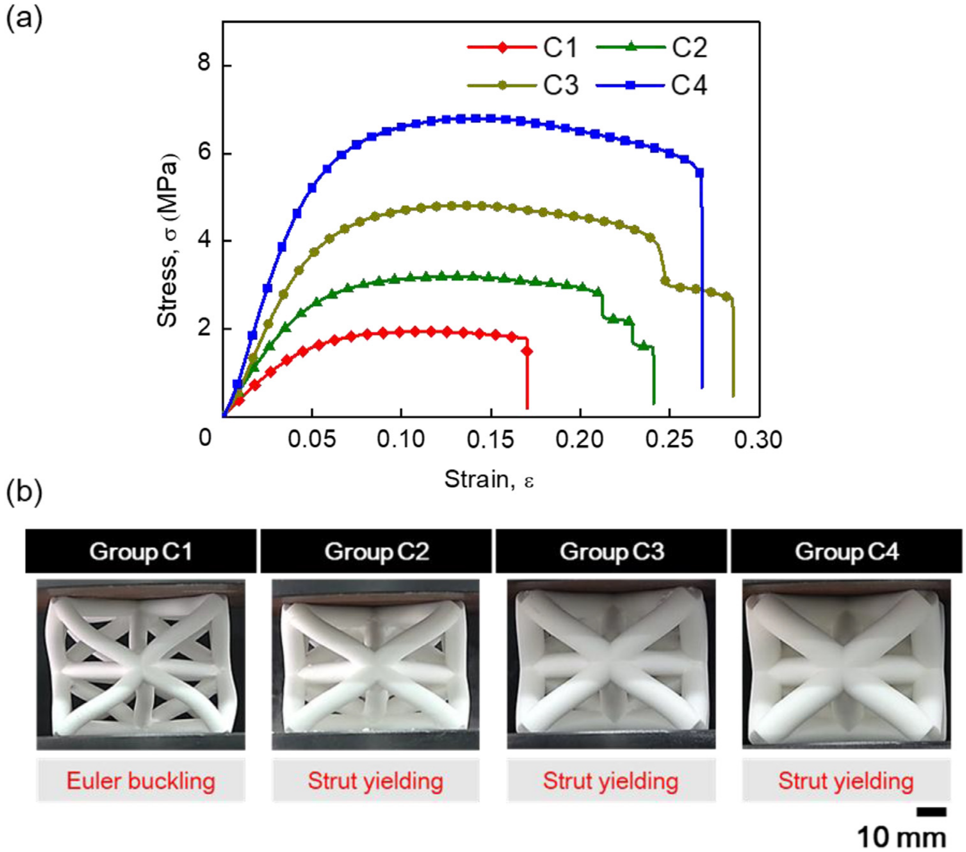

Fig. B1. (a) Compressive stress-strain curves and (b) the corresponding failure modes of the 1st order octet-truss units termed as C1–C4.

A1-A4 (see Table D1), it can be deduced that layer number of the 1st order octet-truss lattice materials will not significantly affect the compressive properties and dominate failure mode, although diagonal crushing or shear localization band appear after the initial failure of multi-layer non-hierarchical lattice materials.

Appendix C. Analytical models for compressive properties of non-hierarchical lattice materials

The mechanical properties of non-hierarchical octet-truss lattice materials with low relative density have been analyzed by Deshpande et al. [35]. Their model, termed the ideal model, however, pertains to micro-scale structures consisting of slender struts, and is thus not appropriate for our nanometer-scale structures with stubby struts (mainly due to strut aspect ratio limitation in nanofabrication) [36].

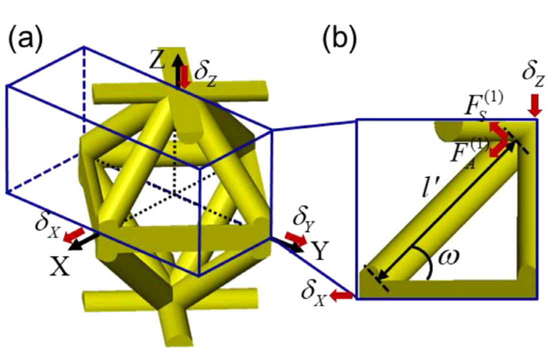

Fig. C1. (a) Free body diagram for the unit cell of the 1st order lattice material; (b) loading condition of a single strut.

The relative densities of our 1st order lattice material, described in the experimental section of the main paper, range from 0.15 to 0.42. For specimens with such high relative density, the nodal volume effect and bending deformation effects are both included in the following modified analytical models. The corresponding free body diagram of octet-truss unit cell is shown in Fig. C1, as employed in previous studies [36, 42].

(1). Stiffness

The deformation of a single strut is analyzed by considering the lateral displacement δ_X, δ_Y, as shown in Fig. C1-b. Applying a z-displacement δ_Z to a octet unit cell, the lateral displacements in the x and y directions have $\delta_X = \delta_Y = \delta_Z/3$ according to our previous study which considered the Poisson's effect [36]. Taking stretching and bending deformation into account, the axial and shear force, $F_A^{(1)}$ and $F_S^{(1)}$, in the strut can be given by Timoshenko beam theory [43] as:

$$F_A^{(1)} = \frac{E_S \pi d_1^2 (\delta_Z \sin\omega - \delta_X \cos\omega)}{4 l_1{}'}, \tag{B1}$$

$$F_S^{(1)} = \frac{12 P_T^{(1)} E_S I_1 (\delta_Z \cos\omega + \delta_X \sin\omega)}{l_1{}'^3}, \tag{B2}$$

where ω is strut inclined angle; $l_1{}' = l_1 - \sqrt{2} d_1$ is the equivalent length depending on the nodal volume of struts in lattices, and I_1 is the inertia moment of area of the beam cross section, given by $I_1 = \pi d_1^4/64$. $P_T^{(1)} = 1/(1 + 12 E_S I_1/\kappa G A_1 l_1{}'^2)$ is the shear modification of Timoshenko beam, where κ is shear coefficient, G is shear modulus and $A_1 = \pi d_1^2/4$ is the cross-section area of the 1st order strut. For a circular beam, $\kappa = (6 + 12\nu + 6\nu^2)/(7 + 12\nu + 4\nu^2)$, where ν is the Poisson's ratio of the material [44].

Table D1
Theoretical compressive stiffness and strength of the 1st order lattice materials, compared to experimental values. Ideal: models considering neither nodal volume effect nor bending effect; N: nodal volume effect only; B: bending effect only; N + B: considering both nodal volume and bending effects; n represents the boundary condition at the strut ends with $n = 1$ for pin-joined and $n = 2$ for fixed-end.

Specimen	Stiffness (MPa, by theory)				Stiffness	Deviation percentage
	Ideal	N	B	N + B	(MPa, by tests)	
A1	22.82	**29.50**	24.19	31.26	28.6	3.05%
A2	35.66	49.72	39.30	**54.79**	53.7	1.99%
A3	51.35	77.73	59.43	**89.96**	98.7	9.72%
A4	69.89	115.71	85.61	**141.73**	145	2.31%

Specimen	Strength (MPa, by theory) Euler Buckling (EB)								Strength (MPa, by tests)	Failure mode	Deviation percentage
	Pin-jointed ($n = 1$)		Fixed-end ($n = 2$)				Plastic Yielding (PY)				
	Ideal	N	Ideal	N	B	N + B	N	N + B			
A1	1.10	**1.84**	4.41	7.37	4.677	7.81	2.18	2.31	1.60	**EB**	13.04%
A2	2.69	5.24	10.77	20.95	11.87	23.08	**3.40**	3.75	3.14	**PY**	7.65%
A3	5.58	12.80	22.34	51.19	25.85	59.24	4.90	**5.67**	5.27	**PY**	7.05%
A4	10.35	28.36	41.39	113.43	50.69	138.94	6.66	**8.16**	8.09	**PY**	0.86%

Accordingly, the compressive stiffness $E_Z^{(1)}$ under uniaxial compression can be deduced to be:

$$E_Z^{(1)} = \frac{\sqrt{2}\pi d_1^2}{6 l_1^2} E_S \lambda_N^{(1)} \lambda_B^{(1)}, \tag{B3}$$

where $\lambda_N^{(1)} = l_1/l_1{}'$ and $\lambda_B^{(1)} = 1 + 1.5 P_T^{(1)} (d_1/l_1{}')^2$ represent the contribution by the nodal volume effect and bending deformation effect, respectively. Note that the nodal volume and bending effects are first- and second-order quantities of d_1/l_1, and can be neglected as the relative density is small (refer to a slender lattice truss with small d_1/l_1).

(2). Strength

A stretching-dominated lattice structure may fail by Euler buckling or plastic yielding under compressive loading, depending on the d_1/l_1 ratio of the lattice struts. Accordingly, the corresponding failure strength $\sigma_Z^{(1)}$ for the 1st order octet-truss lattice materials can be given by:

$$\sigma_Z^{(1)} = \begin{cases} \sigma_{buckling}^{(1)} = \dfrac{\sqrt{2} n^2 \pi^3 d_1{}^4}{32 l_1{}^4} E_S \left(\lambda_N^{(1)}\right)^2 \lambda_B^{(1)} \text{if } \dfrac{d_1}{l_1} \lambda_N^{(1)} < \sqrt{\dfrac{16\sigma_{ys}}{\pi^2 E_S}}, \\ \sigma_{yielding}^{(1)} = \dfrac{\sqrt{2}\pi d_1^2}{2 l_1^2} \sigma_{ys} \lambda_B^{(1)} \text{if } \dfrac{d_1}{l_1} \lambda_N^{(1)} \geq \sqrt{\dfrac{16\sigma_{ys}}{\pi^2 E_S}}. \end{cases}, \tag{B4}$$

where n is determined by the boundary conditions of lattice struts, with $n = 1$ for pin-joined struts and $n = 2$ for fixed-end struts. Note that the nodal volume effect $\lambda_N^{(1)}$ equals unity in the expression of $\sigma_{yielding}^{(1)}$, because the modification of $l_1{}'$ can be offset by the axial stress.

Appendix D. Comparison of theoretical and experimental compressive stiffness and strength values

The theoretical and experimental values of compressive stiffness and strength for the 1st and 2nd order octet-truss lattice materials are summarized in Tables D1 and D2, respectively. Effects of nodal volume and bending effects on the accuracy of prediction results are outlined, with the bold values in Tables D1 and D2 corresponding to the most appropriate analytical models that can best predict the experimental data.

For all the non-hierarchical lattice material in the present study, we find that the nodal volume effect must be considered in the theoretical models to better predict the compressive stiffness and strength values. In addition, for samples with the lowest relative density of 0.15 (Group A1) which fail by Euler buckling, our predicted theoretical values agree well with the experimental stiffness and strength values when effects of bending deformation are not included; conversely, for samples with larger relative densities greater than 0.2 (Group A3-A4), both nodal and

Table D2
Theoretical compressive stiffness and strength of the 2nd order lattice materials, as compared to experimental values.

Specimen	Stiffness (MPa, by theory)		Stiffness (MPa, by tests)	Deviation percentage
	Ideal	N		
B1	2.67	**4.77**	4.02	15.72%
B2	4.18	**8.04**	7.9	1.74%
B3	6.02	**12.56**	14.1	12.26%
B4	8.19	**18.70**	20.1	7.49%
B5	7.43	**16.36**	18.72	14.43%
B6	2.67	**4.78**	4.5	5.86%

Specimen	Strength (MPa, by theory)					Strength (MPa, by tests)	Failure mode	Deviation percentage
	Euler buckling of smaller strut (EB1)		Euler buckling of larger strut (EB2)		plastic Yielding (PY)			
	Ideal	N	Ideal	N	N			
B1	**0.13**	0.22	0.13	0.24	0.25	0.09	**EB1**	30.77%
B2	0.32	0.61	0.20	**0.38**	0.40	0.3	**EB2**	21.05%
B3	0.65	1.50	0.29	**0.55**	0.57	0.53	**EB2**	3.64%
B4	1.21	3.32	0.39	**0.75**	0.78	0.96	**EB2**	28.00%
B5	0.56	1.09	0.62	1.55	**0.71**	0.82	**PY**	15.49%
B6	0.20	0.39	0.08	**0.13**	0.25	0.175	**EB2**	34.62%

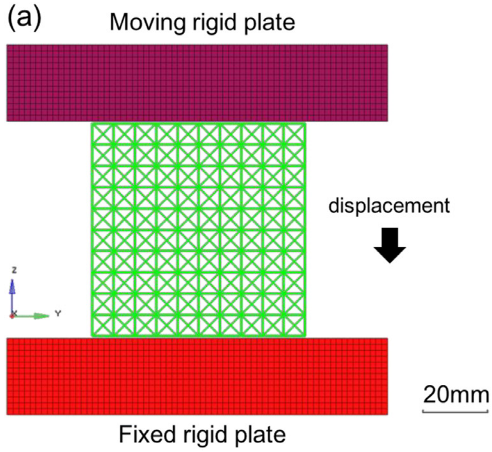

Fig. E1. Simulation models illustrated with the loading condition for (a) the 1st order octet truss lattice material, and (b) the 2nd order octet truss lattice material.

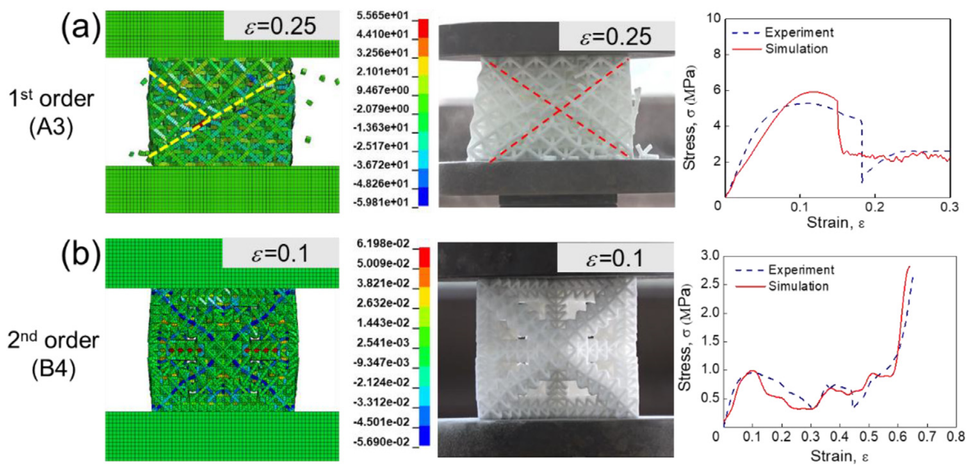

Fig. E2. Comparison of numerical simulations with experimental results for failure modes at a specific strain during compressive stress-strain curves, shown for (a) 1st order octet-truss lattice materials (A3), and (b) 2nd order octet-truss lattice materials (B4).

bending effects need to be considered for the most accurate theoretical predictions. However, Group A2 with medium relative density appear to be more sensitive to strut end boundary conditions, which can sometimes lie within the transition area of pin-jointed and fixed-end conditions ($1 < n < 2$); because of this, our models that respectively include or exclude the slight contribution from bending deformation can provide better predictions of the compressive stiffness and strength of Group A2. Generally, accurate consideration of the nodal volume effect provides the most enhancement to predictions of the ideal model; we regard the nodal volume effect as a first-order trivial quantity, as compared to the bending effect which is deemed to be a second-order small quantity.

For all the 2nd order hierarchical lattice material, models including nodal volume effects of both smaller and larger lattice members can provide an accurate prediction of the compressive stiffness. For samples in Group B1 with the lowest relative density of 0.05, models which exclude any nodal volume effect provide better predictions of experimental strength values. However, for samples with larger relative densities, better predictions are found when the nodal volume effect is included, although prediction still deviate from experimental data (see Table D2). We attribute this deviation to our simplified calculation of the buckling resistance of larger struts (Eq. 5). Overall, the appropriate model for accurate prediction of the mechanical properties of our hierarchical lattice materials is primarily dependent on geometry.

Appendix E. Simulation

Numerical simulation was performed to further investigate the accuracy of appropriate theoretical models on predicted mechanical properties and failure modes of our architected materials. Using the LS-DYNA finite element program, quasi-static compression performance was simulated, with results shown in Fig. E1 for non-hierarchical and second-order hierarchical octet-truss lattice materials with various slenderness ratios from the two structural levels. During the simulation, circular lattice struts were modeled using Hughes-Liu beam elements. An elasto-plastic material model with maximum plastic failure strain criterion was employed here. After convergence analysis, the mesh size was set to be 0.625 mm for the non-hierarchical lattice material and 1.1 mm for the 2nd order hierarchical one. Automatic node to surface contact was defined between the lattice and plates, while automatic general contact was defined for the self-interaction of lattice struts. An implicit-explicit switch method was utilized in this work, which was proved to be more efficient and accurate compared with either implicit-only or explicit-only methods. Specifically, the whole compression process was simulated through an implicit algorism initially until collapse, and then the solver was automatically switched to an explicit algorism for higher calculation efficiency.

The numerical models were validated by comparison to experimental results. As shown in Fig. E2, the numerical simulations of the compressive response were compared with those measured by experiments. For the 1st order lattice material shown Fig. E2-a, the elastic region and initial collapse strength obtained by numerical simulations (solid red curves) match well with the experimental results (dashed yellow curves). The maximum deviation of peak stresses is 12.3%. Nevertheless, the stress-strain curves obtained by simulation are systematically lower than experimental results in the plateau region, which is attributed to an inappropriate treatment of damage evolution in the current beam element model. For the 2nd order lattice material in Fig. E2-b, the numerical stress-strain curves (solid blue curves) accurately predict the trend of the stress-strain history from the elastic to densification regions. The maximum deviation of initial collapse strength is 10.0%. It should be noted here that a good agreement between simulation and experiment is seldom seen when there is a sharp decline in stress due to the abrupt collapse of lattice struts. However, in general, the comparison of numerical predictions and experimental results indicate that the finite element analysis developed here is quite reliable for both 1st and 2nd order lattice materials described in this work. Simulations for structures with more varied geometries could be carried out in the future to aid in the selection of even more appropriate theoretical models.

References

[1] Fratzl P, Weinkamer R. Nature's hierarchical materials. Prog. Mater. Sci. 2007;52:1263–334.
[2] Robinson WJ, Goll RM. Fine Skeletal Structure of the Radiolarian Callimitra carolotae Haeckel. Micropaleontology 1978;24:432–9.
[3] Weiner S, Wagner HD. THE MATERIAL BONE: Structure-Mechanical Function Relations. Ann. Rev. Mater. Res. 1998;28:271–98.
[4] Aizenberg J, Weaver JC, Thanawala MS, Sundar VC, Morse DE, Fratzl P. Skeleton of Euplectella sp.: Structural Hierarchy from the Nanoscale to the Macroscale. Science 2005;309:275–8.
[5] Queheillalt DT, Wadley HNG. Hollow pyramidal lattice truss structures. Int. J. Mater Res. 2013;102:389–400.
[6] Wang B, Wu L, Ma L, Sun Y, Du S. Mechanical behavior of the sandwich structures with carbon fiber-reinforced pyramidal lattice truss core. Mater. Des. 2010;31:2659–63.
[7] Wang S, Wu L, Ma L. Low-velocity impact and residual tensile strength analysis to carbon fiber composite laminates. Mater. Des. 2010;31:118–25.
[8] Xiong J, Ma L, Pan S, Wu L, Papadopoulos J, Vaziri A. Shear and bending performance of carbon fiber composite sandwich panels with pyramidal truss cores. Acta Mater. 2012;60:1455–66.
[9] Wang P, Fan H, Xu B, Mei J, Wu K, Wang H, He R, Fang D. Collapse criteria for high temperature ceramic lattice truss materials. Appl. Therm. Eng. 2015;89:505–13.
[10] Bonatti C, Mohr D. Large deformation response of additively-manufactured FCC metamaterials: From octet truss lattices towards continuous shell mesostructures. Int. J. Plast. 2017;92:122–47.
[11] Ozdemir Z, Hernandez-Nava E, Tyas A, Warren JA, Fay SD, Goodall R, Todd L, Askes H. Energy absorption in lattice structures in dynamics: Experiments. Int. J. Impact Eng. 2016;89:49–61.
[12] Xiao L, Song W, Wang C, Liu H, Tang H, Wang J. Mechanical behavior of open-cell rhombic dodecahedron Ti–6Al–4V lattice structure. Mater. Sci. Eng A-Struct. Mater. 2015;640:375–84.
[13] Tancogne-Dejean T, Spierings AB, Mohr D. Additively-manufactured metallic micro-lattice materials for high specific energy absorption under static and dynamic loading. Acta Mater 2016;116:14–28.
[14] Cao X, Duan S, Liang J, Wen W, Fang D. Mechanical properties of an improved 3D-printed rhombic dodecahedron stainless steel lattice structure of variable cross section. Int. J. Mech. Sci. 2018;145:53–63.
[15] Zhang M, Yang Z, Lu Z, Liao B, He X. Effective elastic properties and initial yield surfaces of two 3D lattice structures. Int. J. Mech. Sci. 2018;138-139:146–58.
[16] Yuan S, Shen F, Bai J, Chua CK, Wei J, Zhou K. 3D soft auxetic lattice structures fabricated by selective laser sintering: TPU powder evaluation and process optimization. Mater. Des. 2017;120:317–27.
[17] Compton BG, Lewis JA. 3D printing: 3D-printing of lightweight cellular composites. Adv. Mater. 2014;26:5930–5.
[18] Yin S, Li J, Liu B, Meng K, Huan Y, Nutt S, Xu J. Honeytubes: Hollow lattice truss reinforced honeycombs for crushing protection. Compos. Struct. 2017;160:1147–54.
[19] Han SC, Lee JW, Kang K. A New Type of Low Density Material: Shellular. Adv. Mater. 2015;27:5506–11.
[20] Jacobsen AJ, Barvosa-Carter W, Nutt S. Micro-scale truss structures with three–fold and six-fold symmetry formed from self-propagating polymer waveguides. Acta Mater. 2008;56:2540–8.
[21] Jacobsen AJ, Barvosa-Carter W, Nutt S. Shear behavior of polymer micro-scale truss structures formed from self-propagating polymer waveguides. Acta Mater. 2008;56:1209–18.
[22] Yin S, Jacobsen AJ, Wu L, Nutt S. Inertial stabilization of flexible polymer micro-lattice materials. J. Mater. Sci. 2013;48:6558–66.
[23] Zheng X, Lee H, Weisgraber TH, Shusteff M, Deotte J, Duoss EB, Kuntz JD, Biener MM, Ge Q, Jackson JA, Kucheyev SO, Fang NX, Spadaccini CM. Ultralight, ultrastiff mechanical metamaterials. Science 2014;344:1373–7.
[24] Zheng X, Smith W, Jackson J, Moran B, Cui H, Chen D, Ye J, Fang N, Rodriguez N, Weisgraber T, Spadaccini CM. Multiscale metallic metamaterials. Nat. Mater. 2016;15(10):1110.
[25] Bauer J, Meza LR, Schaedler TA, Schwaiger R, Zheng X, Valdevit L. Nanolattices: An Emerging Class of Mechanical Metamaterials. Adv. Mater. 2017:1701850.
[26] Ajdari A, Jahromi BH, Papadopoulos J, Nayeb-Hashemi H, Vaziri A. Hierarchical honeycombs with tailorable properties. Int. J. Solids Struct. 2012;49:1413–19.
[27] Banerjee S. On the mechanical properties of hierarchical lattices. Mech Mater. 2014;72:19–32.
[28] Oftadeh R, Haghpanah B, Vella D, Boudaoud A, Vaziri A. Optimal fractal-like hierarchical honeycombs. Phys. Rev. Lett. 2014;113:104301.
[29] Zhang Y, Xu X, Wang J, Chen T, Wang C. Crushing analysis for novel bio-inspired hierarchical circular structures subjected to axial load. Int. J. Mech. Sci. 2018;140:407–31.
[30] Oftadeh R, Haghpanah B, Papadopoulos J, Hamouda AMS, Nayeb-Hashemi H, Vaziri A. Mechanics of anisotropic hierarchical honeycombs. Int. J. Mech. Sci. 2014;81:126–36.
[31] Xu H, Farag A, Pasini D. Multilevel hierarchy in bi-material lattices with high specific stiffness and unbounded thermal expansion. Acta Mater. 2017;134:155–66.
[32] Rayneau-Kirkhope D, Mao Y, Farr R. Ultralight fractal structures from hollow tubes. Phys. Rev. Lett. 2012;109:204301.
[33] Vigliotti A, Pasini D. Mechanical properties of hierarchical lattices. Mech Mater. 2013;62:32–43.
[34] Meza LR, Zelhofer AJ, Clarke N, Mateos AJ, Kochmann DM, Greer JR. Resilient 3D hierarchical architected metamaterials. Proc Natl. Acad. Sci. U.S.A. 2015;112:11502–7.
[35] Deshpande VS, Fleck NA, Ashby MF. Effective properties of the octet-truss lattice material. J. Mech. Phys. Solids 2001;49:1747–69.
[36] He Z, Wang F, Zhu Y, Wu H, Park HS. Mechanical properties of copper octet-truss nanolattices. J. Mech. Phys. Solids 2017;101:133–49.
[37] ASTM: D695-15. Standard test method for compressive properties of rigid plastics. Weat Conshohocken (PA): ASTM Int.; 2015.
[38] ASTM: D638-14. Standard test method for tensile properties of plastics. Weat Conshohocken (PA): ASTM Int.; 2014.
[39] Wicks N, Hutchinson JW. Optimal truss plates. Int. J. Solids Struct. 2001;38:5165–83.
[40] Fleck NA, Sridhar I. End compression of sandwich columns. Compos Pt A-Appl Sci Manuf 2002;33:353–9.
[41] Yin S, Wu L, Nutt S. Stretch–bend-hybrid hierarchical composite pyramidal lattice cores. Compos. Struct. 2013;98:153–9.
[42] Dong L, Deshpande V, Wadley H. Mechanical response of Ti–6Al–4V octet-truss lattice structures. Int. J. Solids Struct. 2015;60–61:107–24.
[43] Xia R, Li X, Qin Q, Liu J, Feng X. Surface effects on the mechanical properties of nanoporous materials. Nanotechnology 2011;22:265714.
[44] Hutchinson JR. Shear Coefficients for Timoshenko Beam Theory. J. Appl. Mech. 2001;68:87–92.